sPH-HF-2017-001
Heavy Flavor Jet Simulation and Analysis

The sPHENIX Collaboration

Version v1.1, July 9, 2017

Abstract

This analysis note summarizes the heavy flavor (HF) jet studies performed by the sPHENIX HF topical group. We demonstrate the capability of tagging b-jet in p+p and central Au+Au collisions at $\sqrt{s_{NN}} = 200$ GeV, using GEANT4 simulation of sPHENIX detector. A Monolithic Active Pixel Sensor Vertex Detector (MVTX) upgrade to sPHENIX is critical in enabling the b-jet capability. The projections for b-jet nuclear modification and di-b-jet correlations are then presented. The progress of exploring the b-jet-B-meson correlations is also discussed.

Contents

Chapter 1

Introduction

1.1 Physics Goals

Heavy flavor (HF) quarks (c, b) play a unique role for studying QCD in vacuum as well as in quarkgluon plasma (QGP) [4]. Their masses are much larger than the QCD scale, the additional QCD masses due to chiral symmetry breaking, and the typical QGP temperature reached at RHIC and LHC. Therefore they are created predominantly from initial hard scatterings and their production rates are calculable in perturbative QCD [8, 7]. They are thus calibrated probes that can be used to study the QGP in a controlled manner. In addition, when compared with the light quarks and gluons, heavy quark probes may provide differential sensitivity to collision and radiative partonic energy loss in the QGP, and therefore provide stringent test of models describing the transport properties of QGP [5, 13].

The planned sPHENIX baseline detectors [2] with the proposed Monolithic Active Pixel Sensor Vertex Detector (MVTX) upgrade [16] will enable new heavy-flavor physics capability in QGP studies, extending present RHIC measurements to much broader transverse momentum range and providing access to critical but uncharted part of QGP parameter space. In combination with the sPHENIX calorimetric jet reconstruction, the sPHENIX and MVTX provide a particularly important new capability to sPHENIX baseline program - the identification of jets originating from heavy quarks for p_T = 15–40 GeV/c. In this note, we investigate the detection capability and physics reach of the b-jet program at sPHENIX via simulation and reconstruction. This particular measurement represents both a new opportunity at RHIC and an example of complementarity to the LHC. The projected sPHENIX measurement extends the LHC measurement [11, 12] to lower transverse momenta and provides a kinematic overlap, where the same jets can be studied in the different QGP conditions at RHIC and LHC.

Compared to HF hadrons, measurements of jets provide more information on the parton kinematics and the nature of parton interactions with the QGP

medium. The evolution of parton showers probes the coupling with the medium over a range of scales, providing sensitivity to its scale-dependent microscopic structure. Jets containing b-quarks (b-jets) are of particular interest, as bottom quarks, which are $\sim$1000 times heavier than the light quarks, produce unique energy loss signatures due to their large mass (4.2 GeV/c^2) [19]. At momenta comparable to the b-quark mass scale, bottom quarks may preferentially lose energy via collisions with the plasma quasi-particles and not via gluon radiation, which is predominant for light quarks [5, 13].

Measurements of b-jets in Pb+Pb collisions at LHC cover momenta larger than 80 GeV/c [11, 12]. Intriguingly, these measurements indicate a nuclear modification factor very similar to inclusive jets [11]. One of the explanations is that the mass of the b-quark is small when compared with the jet transverse momenta, $p_T \geq 80$ GeV/c. The other hypothesis is that 30-70% of b-jets at LHC in $p_T = 50 - 1000$ TeV/c are from gluon splitting processes [6, 23], for which jet containing a b-quark still behaves as a massive color octet object when crossing the medium, resembling a massive gluon [14]. In comparison to LHC, measurements at RHIC will be both complementary by probing different QGP conditions, but also provide the following distinct advantages:

- b-jets can be measured with momentum as low as 15 GeV/c, where the quark mass is more important for the energy loss mechanisms.
- The main processes producing b-jets at RHIC are the leading order gluon fusion ($g + g \rightarrow b + \bar{b}$) and excitation of intrinsic b-quarks in the proton wave function ($b + g \rightarrow b + g$). Therefore, b-jet at RHIC are less contaminated by the gluon splitting channel, which is estimated to be below 15% using PYTHIA8 simulations [2].

1.2 Detector Setup

In this section, we discuss the relevant aspects of the sPHENIX detector configuration and performance. The sPHENIX experiment [2] consists of tracking and calorimetry detectors, built around a 1.4 T super conductor magnet and covering full azimuth in $|\eta| < 1.1$. The whole detector system will take data at 15 kHz, which is much higher than the current RHIC experiments such as PHENIX and STAR.

1.2.1 Tracking

The tracking detectors include following subsystems from inner radius to outer:

1. MVTX (alternatively noted as MAPS), which consists of three layers of silicon pixel trackers
2. Intermediate tracker (INTT or IT), which consists of four layers of silicon pixel trackers

3. Time projection chamber (TPC), which consists of 40 layers of silicon pixel trackers. In this note, a previous configuration of 60-layer TPC configuration is used, which occupies the same radial space. For vertex measurement that this note is sensitive to, the difference between the two configurations of TPC layers is small.

In particular, the MVTX, as shown in Figure 1.1, is the key upgrade to sPHENIX enabling precision measurements of the primary vertex as well as the displaced secondary tracks from heavy quark decays. A full detector GEANT4 display is also shown in Figure 1.2.

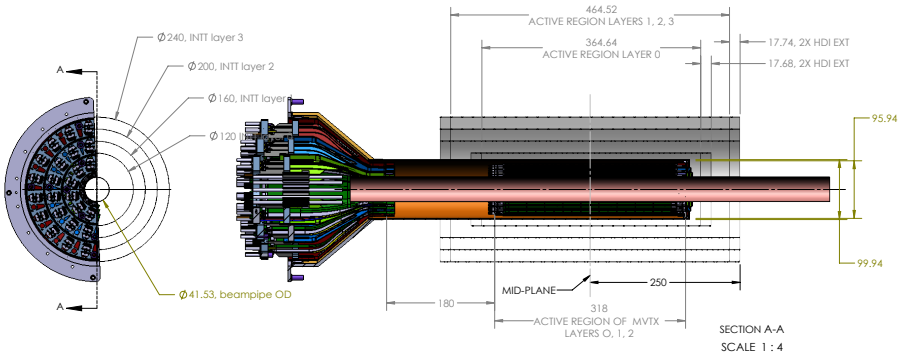

Figure 1.1: sPHENIX vertex detectors. Beam view of MVTX detector on the left, and side view of MVTX and INTT on the right.

In this note, we use a cylindrical approximation to the full tracking detector geometry. The proper material budget and pixel size are assigned to each layer to reproduce the average multiple scattering and cluster position resolution at each tracking layer. A Hough-transform based pattern recognition and Kalman-filter based track fitting algorithms were employed for track finding and fitting, respectively.

Figure 1.3 shows the single track efficiency and the DCA pointing resolution in the bending plane as a function of p_T based on the full GEANT4 detector simulation plus the offline tracking software reconstruction. The efficiencies were evaluated using charged pion tracks embedded in central HIJING Au+Au events (i.e., highest multiplicity in sPHENIX). The single track efficiency is about 80% at 1 GeV/c and the DCA pointing resolution is about 40 μm for 0.5–1 GeV/c tracks. These performance parameters meet the requirements for the proposed measurements.

The collaboration is finalizing on a new tracking simulation setup, which employs full ladder-based geometry for the MVTX and INTT subdetectors in GEANT4 and GENFIT2-based [22] pattern recognition and fitting modules. Although it is not yet used in b-jet simulation study of this note, we expect

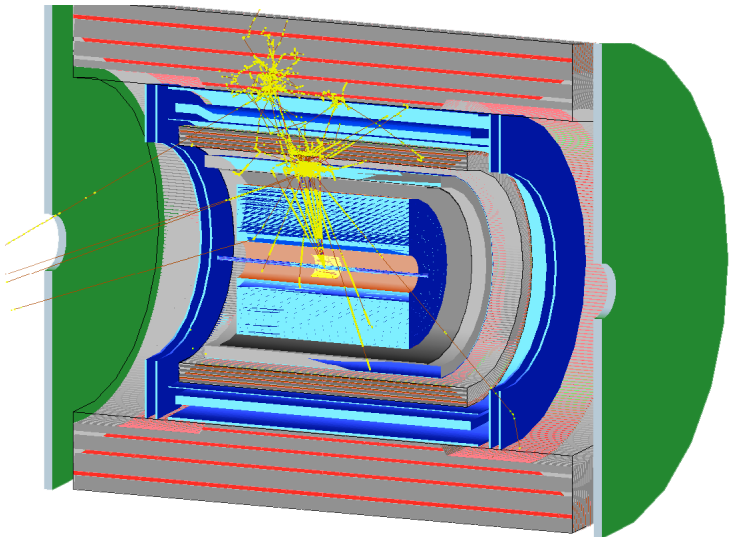

Figure 1.2: Side view of the sPHENIX detector in GEANT4 and a $p_T = 30\,\mathrm{GeV}/c$ B-meson showers. Only half of the detector is displayed to show the inner subdetectors.

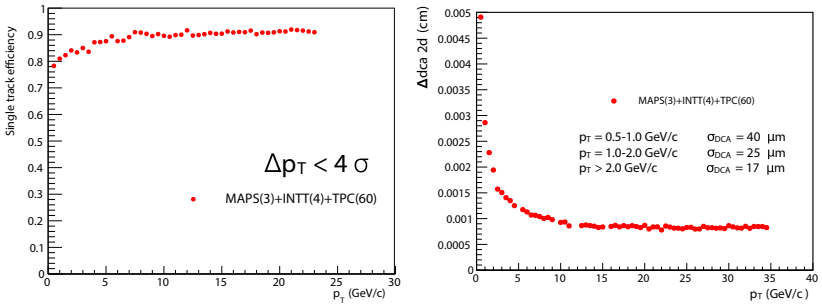

Figure 1.3: Single track reconstruction efficiency (left) and DCA pointing resolution in the bending plane (right) in central Au+Au collisions from full HIJING plus GEANT4 simulation.

this new simulation be employed for b-jet studies soon and provide improved simulation and performance.

1.2.2 Calorimetry

The sPHENIX calorimeter system includes an electromagnetic calorimeter and an inner hadronic calorimeter, which sit inside a solenoid coil, and an outer hadronic calorimeter located outside of the coil [2]. The three layers of calorimeter allow the calorimetry-based measurement of jets at RHIC with an energy

resolution of $\Delta E/E = 120\%/\sqrt{E}$ and provides containment for 80% of opposite di-jet pairs from the same hard collision. The triggering system is also designed to provide jet-patch triggers by requiring the minimal energy sum from combinations of calorimeter towers which belong to the same jet-cones. Furthermore, the electromagnetic calorimeter provides for the triggering, identification and measurement of high-energy electrons with an energy resolution better than $\Delta E/E = 15\%/\sqrt{E}$.

In the current iteration of b-jet studies, we assumed the factorization of the tracking-centralized b-jet tagging and the calorimetry-centralized jet finding, and focused on the former aspect. Therefore, all jets from this note is found by applying the anti-k_T algorithm on the PYTHIA8 event records, while the tracks are found by reconstructing the GEANT4 simulation of the full tracking detectors. The effects of fake calorimetry jets and the interplay between jet-finding and b-jet-tagging will be studied in the further iterations of b-jet simulations.

1.3 Luminosity and acceptance assumptions

The five-year sPHENIX run plan, as lined out in note sPH-TRG-2017-001 [17], is used for projection in this note, which includes the following collision systems:

- p+p,$\sqrt{s} = 200$ **GeV:** sampling 200 pb^{-1} with jet patch trigger, which is rounded up from 197 pb^{-1} as in sPH-TRG-2017-001 [17].
- **Au**+**Au**,$\sqrt{s} = 200$ **GeV:** for b-jets with $p_T < 30$ GeV/c, we assume 240 Billion MB Au+Au collision, which is rounded up from 239 Billion MB Au+Au collision as in sPH-TRG-2017-001 [17]. For b-jets with $p_T > 30$ GeV/c, we assume 550 Billion Au+Au collision sampled using a jet patch trigger of moderate rejections.
- p+**Au**,$\sqrt{s} = 200$ **GeV:** 0.33 pb^{-1} with jet patch trigger or 600 billion sampled collisions.

For all collision systems, we use full acceptance for $R = 0.4$ jets in the sPHENIX calorimeter and tracking acceptance of $|\eta_{\text{detector}}| < 1.1$,

$$|\eta_{b\text{-jet}}| < 0.7 (\text{i.e. } 1.1 - R). \tag{1.1}$$

The luminosity projections include the $|v_z| < 10$ cm vertex range, where the MVTX detector provides at least two hits in $|\eta| < 1$, and therefore leads to a full coverage for DCA measurement in the full jet cone.

1.4 Overview for b-jet studies at sPHENIX

The detection of b-jets with the sPHENIX detector is complicated by the comparative rarity of b-jets (Section 2.2), and also by the significant background of the underlying event in heavy ion collisions. Multiple methods have been

explored to demonstrate that the planned sPHENIX detector with the proposed MVTX upgrade allows b-jet tagging, and to enable cross checks of the expected systematic uncertainties. As shown in the right diagram of Figure 1.4, these methods are based on the unique features of B-hadron decays, including the finite decay length and leptonic decay products. In particular, the methods as discussed in this note are as following:

- Identify b-jets by requiring multiple tracks within the jet cone that do not originate from the primary collision vertex. These are likely be the long-lived B-hadron decay products. As an initial study, we performed a full sPHENIX detector simulation to demonstrate this capability as discussed in Section 3.1. Despite the simplified algorithm used in this exploration, the b-tagging performance approaches that seen by CMS in their b-jet analysis at much higher energy [12, 11]. Additional techniques will be deployed in the final software package to further optimize performance, including likelihood analyses, 3-dimensional track displacement and machine learning techniques.

- Identify b-jets by requiring that multiple tracks within the jet cone come from the same displaced secondary vertex distinct from the primary vertex. This method is similar to the previous one except it uses the additional information about the probability of B-hadron decaying into multiple daughter particles. This provides additional power in selecting and cross checking b-jet candidates identified via the first method. We also demonstrated this method in full simulation as discussed in Section 3.2. This method also provides data driven quantification of b-jet purity via secondary vertex kinematics fitting.

After the initial identification of b-jet candidates, the purity of b-jets in the candidate sample will be quantified in a data-driven way using the invariant mass and transverse momentum of the secondary vertex, which has proven to be critically important in the LHC environment [12, 11]. The projected uncertainty of the nuclear modification of inclusive b-jet is shown in Figure 2.2 in Chapter 2, which places stringent tests on the models describing the coupling between heavy quarks and the QGP [14]. We are in close collaboration with theory groups to update the model predictions of inclusive b-jet nuclear modification at the top RHIC Au+Au energy and in the sPHENIX kinematic region.

Beyond the inclusive b-jet nuclear modification measurement, additional techniques in jet substructure and correlation studies will be performed. Inclusive b-jets can originate from a high-energy b-quark (a true b-quark jet) or from a gluon that splits into b-quark and b-antiquark ($g \rightarrow b\bar{b}$-jet). These two categories of b-jets could potentially have very different interactions with the QGP, because in the latter case the correlated b-quark and b-antiquark traverse coherently through the QGP in a color octet state with twice the b-quark mass [14]. Although inclusive b-jets at RHIC are expected to be dominated by the b-quark jets [18], the remaining $g \rightarrow b\bar{b}$-jet component could complicate the interpretation of the inclusive b-jet results.

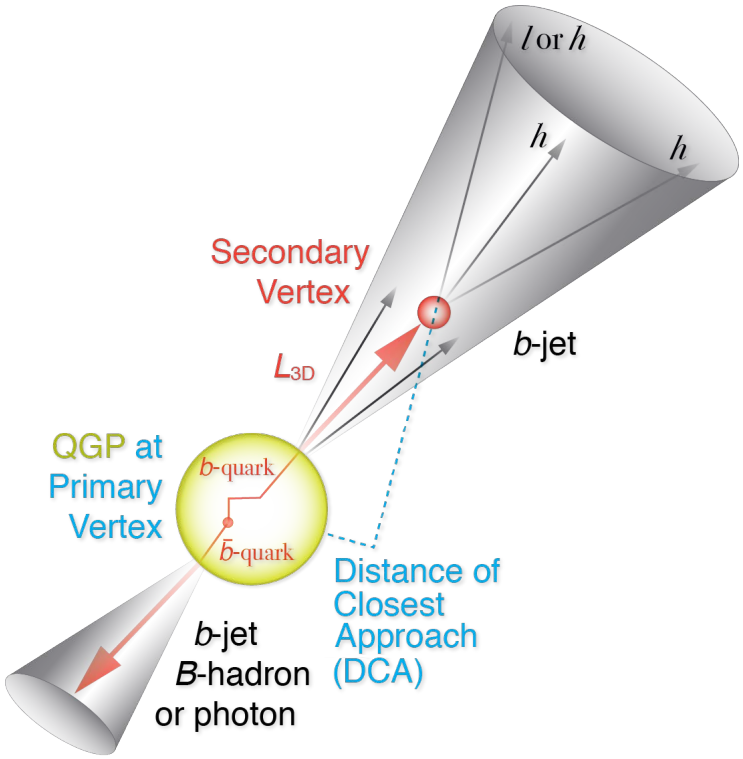

Figure 1.4: A b-quark traverses the QGP and fragments into a b-jet. The principles of tagging the rare b-jets are based on unique features of B-hadrons: long life time and finite decay length of B-hadron (L_{3D} ~few mm), decay tracks from secondary vertices and leptonic decay products.

sPHENIX will allow us to discriminate these two categories of b-jet productions and provide cleaner access to the dynamics of high energy b-quark interactions with the QGP. The fraction of true b-quark jets can also be enhanced by requiring the b-jet candidate to be correlated with another b-jet, B-hadron, or photon in the same event [15], as illustrated in Figure 1.4. In particular, correlations between two b-jets can be measured with high statistics using the MVTX and the sPHENIX detector, taking advantage of their high rate capability and their large instrumented acceptance (covering nearly 80% of produced di-jets [2]). The projection for the transverse momentum balance of b-jet-pairs is discussed in Chapter 4. A preliminary study for b-jet-B-meson correlations is discussed in Chapter 5.

Chapter 2

Event generation and inclusive b-jet projection

2.1 Simulation setup

A PYTHIA8 based simulation using Hard QCD mode [23, 24], $\hat{q}_T = 7$ GeV/c, and `CTEQ6L` PDF [21, 20] was used to simulate the b-jet production rate in sPHENIX. The relevant part of PYTHIA8 configuration file is as following:

```
! phpythia8.cfg for b-jet simulation

! Beam settings
Beams:idA = 2212    ! first beam, p = 2212, pbar = -2212
Beams:idB = 2212    ! second beam, p = 2212, pbar = -2212
Beams:eCM = 200.    ! CM energy of collision

! PDF
PDF:pSet = 7 ! CTEQ6L, NLO alpha_s(M_Z) = 0.1180.

! Process
HardQCD:all = on
! Cuts
PhaseSpace:pTHatMin = 7.0
```

[14] found PYTHIA8 + `CTEQ6L` reproduced the b-jet cross section in LHC data at $\sqrt{s} = 7$ TeV. The b-jet and inclusive jet production rate at the top RHIC Au+Au energy is also checked in Section 2.2.

After the PYTHIA8 simulation, the produced particle goes through truth jet finding, which utilizes the anti-k_T algorithm in FASTJET package with a parameter of $R = 0.4$ [9, 10]. Then, the jet partonic flavor is tagged, which marks the flavor of the jet as the flavor of heaviest quark inside the jet-cone. An alternative definition using heaviest-quark meson inside the jet cone is also available in

the tagger output, but *not* used in this analysis. The tagger setup is committed to the analysis repository at https://github.com/sPHENIX-Collaboration/analysis/tree/master/HF-Jet/TruthGeneration.

A branch of macros repository that execute this setup can be found at https://github.com/blackcathj/macros/tree/SinglePart_master_prod_pythia_truth_Bjet_MB/macros/g4simulations.

2.2 The b-jet cross section

For the cross-section estimation, the equivalent of 53 pb^{-}1 of p+p collisions at$\sqrt{s} = 200$ GeV were simulated using PYTHIA8 with the setup mentioned in Section 2.1. As shown in Figure 2.1, the resulting inclusive jet and b-jet cross section are compared with PHENIX data [3] and FONLL calculations [8, 7], respectively. The fraction of b-jet in the inclusive jet sample of $p_T = 15$–40 GeV/c is approximately 0.5%.

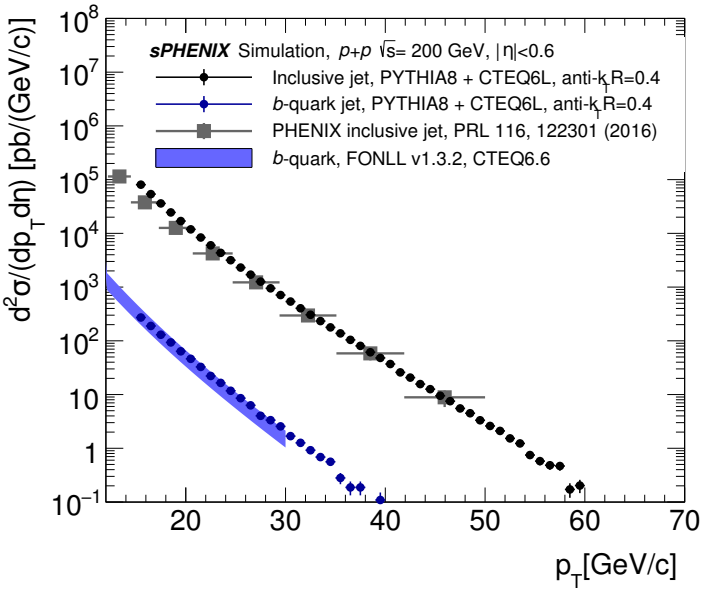

Figure 2.1: Comparison of the cross section for b-jets (blue) and all jets (black). They are consistent with the published inclusive jet cross section [3] and the b-bare-quark production cross section from a FONLL calculations [8, 7], respectively. b-jets are rare compared to the much more abundant light quark jets.

The source code generating this estimation is located at DrawCrossSection() in Draw_HFJetTruth.C as linked here[1]

[1] https://github.com/sPHENIX-Collaboration/analysis/blob/master/HF-Jet/

2.3 The nuclear modification of b-jets

The projected statistical uncertainty for nuclear modification factor in 0-10% Au+Au collisions are shown in Figure 2.2. The jet psuedorapidity is constraint within $|\eta| < 0.7$, which allows full jet cone with $R = 0.4$ be contained within tracking and calorimetry coverage for the full vertex ranges ($|z| < 10$ cm). Based on the b-jet tagging performance studies in Chapter 3, an optimistic but plausible purity of 40% at 60% efficiency in p+p and of 40% purity at 40% efficiency in most central Au+Au collisions are assumed.

Two trigger scenarios are considered:

- Figure 2.2a is assuming untriggered recorded sample of 240 B MB Au+Au collisions.
- Since the uncertainty is only visible for b-jets with $p_T > 30$ GeV/c, a moderate jet trigger is further assumed to allow sampling the full 550 Au+Au collisions in the MVTX vertex range of $|z| < 10$ cm (more in Section 1.3), which leads to Figure 2.2b.

The difference in uncertainty projection between these two scenarios are minor since the uncertainty of R_{AA} for inclusive b-jets are dominated by the p+p statistics. Meanwhile, high Au+Au statistics are highly demanded for the jet correlations measurements as shown in Chapter 4 and 5.

The result shows good statistical precision covering b-jet in kinematics range of $15 < p_T < 40$ GeV/c. This data will provide precision constraint on the b-quark counting constant to QGP as evaluated in a heavy quark transport model [14], which is now reevaluated at RHIC energy under the support of LANL MVTX LDRD program.

The source code generating this estimation is located at `CrossSection2RAA()` in `Draw_HFJetTruth.C` as linked here

`TruthGeneration/macros/Draw_HFJetTruth.C`

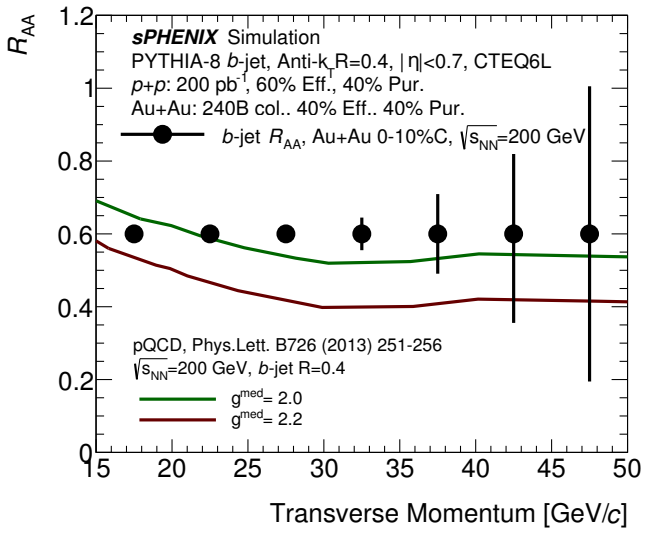

(a)

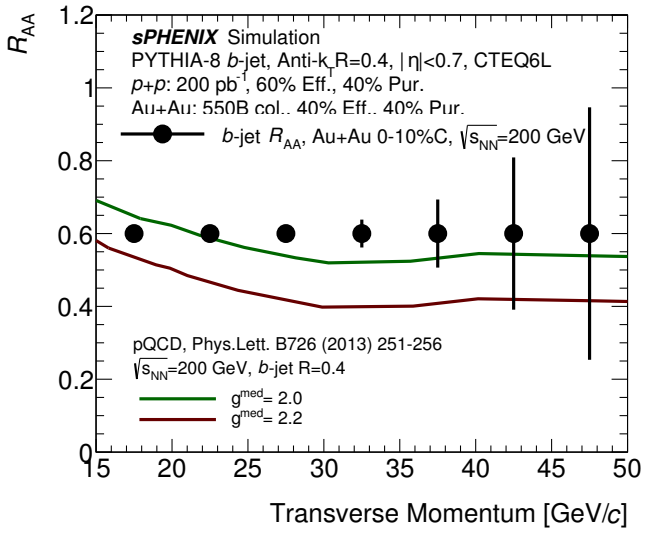

(b)

Figure 2.2: Statistical projection of sPHENIX inclusive b-jet data in terms of the nuclear suppression factor (black circles), which is compared with QGP transport models for b-quark jets evaluated at the RHIC energy with two possible coupling strength (curves) [14]. (a) is assuming untriggered recorded sample of 240 B MB Au+Au collisions, and (b) assumes sampled 550 B Au+Au collisions using a moderate jet trigger.

Chapter 3

The *b*-jet tagging in GEANT4 simulations

The *b*-jet candidates are selected from the inclusive jets samples via the analysis procedures called *b*-jet tagging. Two *b*-jet tagging algorithms have been implemented in a GEANT4 simulation of the full sPHENIX tracking system:

1. The track counting algorithm, which selects *b*-jets by requiring multiple off-vertex tracks inside the jet cone, will be discussed in Section 3.1.

2. The secondary vertex algorithm, which selects *b*-jets by requiring tracks inside the jet cone form vertices displaced from the primary ones, will be discussed in Section 3.2.

These algorithms and their tagging performance will be discussed in this chapter.

3.1 The track-counting algorithm

3.1.1 Introduction

For the track counting method, we identify b-jets by requiring multiple tracks within the jet cone that do not originate from the primary collision vertex. These are likely be the long-lived B-hadron decay products when compared with light-quark jets and c-jets. In this first implementation, we required one, two or three tracks satisfying the significance cut. This algorithm is first developed in the proposal stage of sPHENIX [2], which is now implemented in full GEANT4 tracking simulations. The future version of this algorithm will employ a likelihood method to utilize full information content of tracks.

3.1.2 Simulation and Analysis Setup

As an initial study, we performed a full sPHENIX detector simulation to demonstrate such b-jet tagging capability using the track counting algorithm. The simulation set up includes following components:

- Using generator setup in Section 2.1
- Jet reconstruction: we used the anti-k_T algorithm with a parameter of $R = 0.4$ in the FASTJET package to analyze the generated particles from PYTHIA8.
- Flavor tagging: Using the Jet flavor tagger: `HFJetTruthTrigger` as discussed in Section 2.1
- Tracking: Using cylindrical MVTX(3) + INTT (4) + TPC(60), where numbers in the bracket denote number of layers in each tracking detector. To demonstrate the importance of MVTX upgrade, this study was also performed without MVTX for comparison. The patterThn recognition module used `PHG4HoughTransformTPC`, and track fitting module used `PHG4TrackKalmanFitter`. For DCA calculations, we used RAVE package [1] to reconstruct the primary vertex with option of `avf-smoothing:1` which uses a weight function for tracks based on their standardized distance to the vertex candidate [25, 26].
- The `BJetModule` was used to extract useful information in the DST NodeTrees and create a compact TTree with truth, jet, track information. The plotting macro in the `macros` folder in this package was used to summarize and do the plotting.
- Tracks inside each jet are sorted according to the highest significance of DCA, $DCA/\sigma(DCA)$. A jet is tagged as a b-jet candidate if the one, two or three tracks are above a minimal cut on their significance of DCA, which leads to the performance curve as discussed in the next section.

3.1.3 Results

This section summarize performance results for b-tagging using the track counting algorithm. The tagging performance are quantified as the functions of the rejection of background jet versus b-jet efficiency or functions of b-jet purity versus b-jet efficiency. The background jets included light-quark and gluon jets (l-jets), and charm-jets (c-jets). Two detector configurations are considered, sPHENIX baseline without MVTX in Section 3.1.3, and sPHENIX with the MVTX upgrade in Section 3.1.3.

The b-jet tagging without MVTX

First, we performed b-jet tagging with INTT + TPC only. The results are shown in Figure 3.1 and Figure 3.2.

We could see from Figure 3.2 that even in the relative low occupancy $p+p$ case, the INTT + TPC configuration is far below the targeted $p+p$ working point of 60% efficiency 40% purity. With Au+Au collisions having much higher multiplicity and background, this configuration will provide much lower purity and efficiency. So we do not continue the study for this configuration using Au+Au collisions.

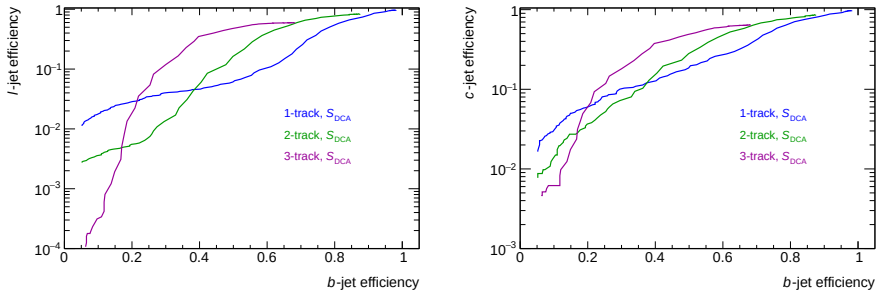

Figure 3.1: For the tracking configuration without the MVTX detector, the l(left)/c(right)-jet efficiency as a function of b-jet tagging efficiency in $p+p$ collisions using the one-, two- and three-large DCA track methods.

The b-jet tagging for sPHENIX with MVTX upgrade

Then we performed the b-jet tagging with the proposed tracking configuration of MVTX+INTT+TPC.

- The tagging performance results in $p+p$ collisions as shown in Figures 3.3 and 3.4.
- Tagging performance with PYTHIA8 jetty events embedded into 0-10% central HIJING Au+Au events are shown in Figures 3.5 and 3.6.

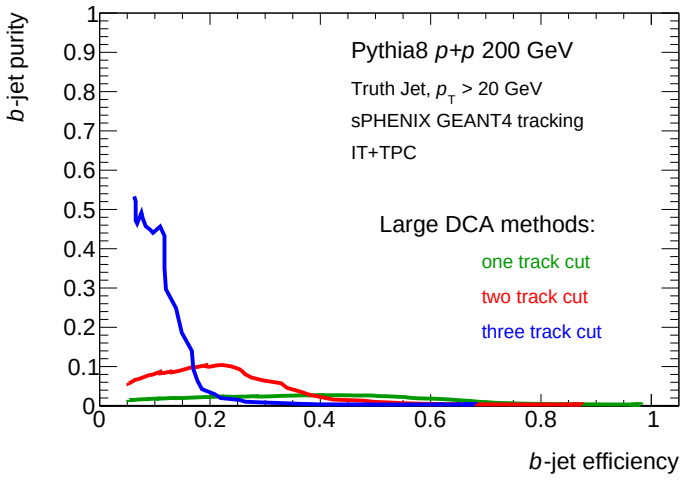

Figure 3.2: For the tracking configuration without the MVTX detector, the b-jet tagging performances in p+p collisions using the one-, two- and three-large DCA track methods. It is far below the targeted p+p working point of 60% efficiency 40% purity.

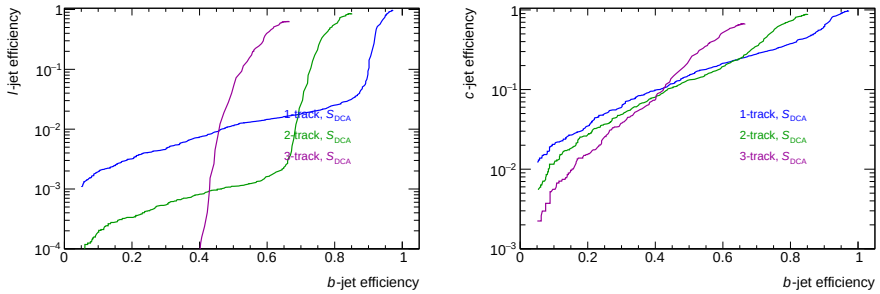

Figure 3.3: Projected l(left)/c(right)-jet efficiency as a function of b-jet tagging efficiency in p+p collisions using the one-, two- and three-large DCA track method with the MVTX detector.

Despite the simplified algorithm used in this study, the b-jet-tagging performance approaches to that of CMS at much higher energy [11]. Additional techniques will be deployed in the final software package to further optimize performance, including likelihood analyses, 3-dimensional track displacement and machine learning techniques.

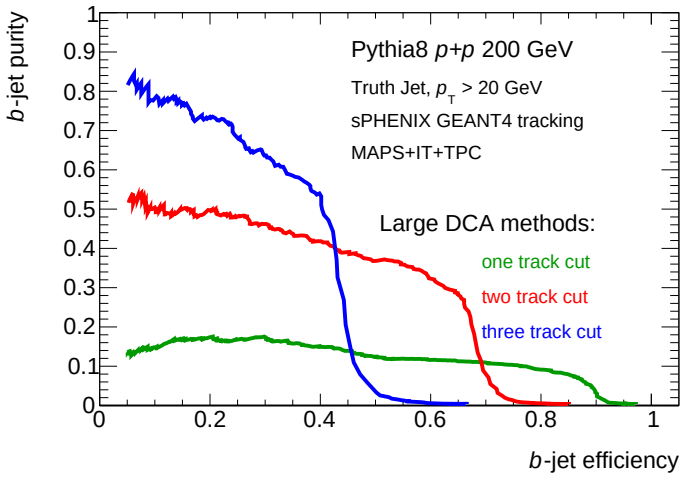

Figure 3.4: Projected b-jet tagging performances in p+p collisions using the multiple large DCA track method.

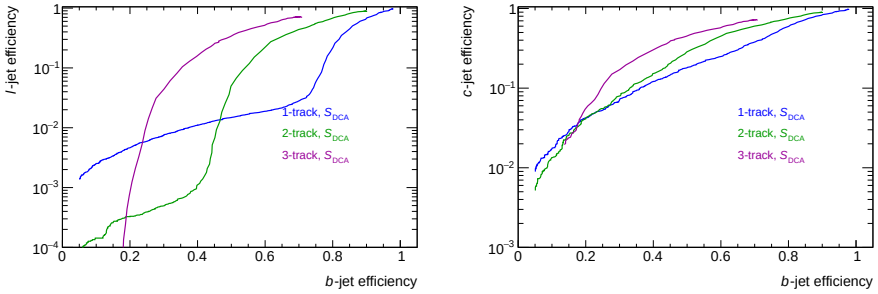

Figure 3.5: l(left)/c(right)-jet efficiency as a function of b-jet tagging efficiency in Au+Au collisions using the one-, two- and three-large DCA track methods with the MVTX detector.

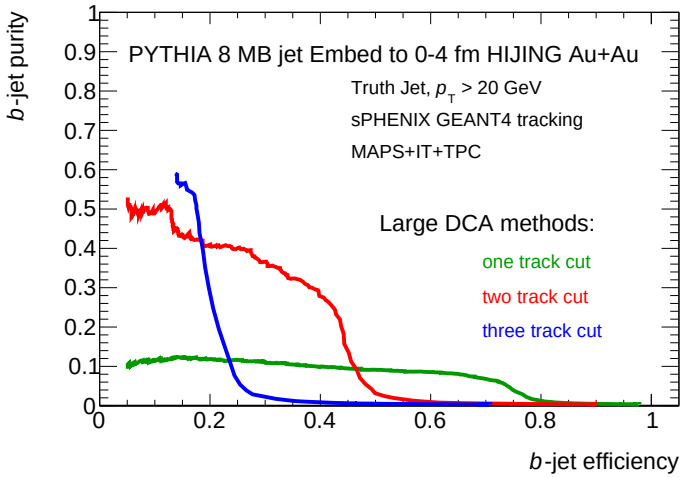

Figure 3.6: b-jet tagging performances in 0-10% central Au+Au collisions using the one-, two- and three-large DCA track methods. The tracking and tagging software is not yet fully optimized. Nevertheless, the performance curves allow an analysis working point of 30-40% purity at 30-40% b-jet efficiency as used in the existing analysis performed at LHC energy [11].

3.2 The secondary vertex algorithm

3.2.1 Introduction

In this section, we identify b-jets by requiring that multiple tracks within the jet cone come from the same displaced secondary vertex distinct from the primary vertex. This method is almost similar to the previous one except it also uses the knowledge that a B-hadron is likely to decay into multiple daughter particles from a displaced common vertex. This provides additional power in selecting and cross checking b-jet candidates identified via the first method. This method is demonstrated in full simulation as discussed in this section. This method also provides data driven quantification of b-jet purity via secondary vertex kinematics fitting.

3.2.2 Simulation and Analysis Setup

As an initial study for sPHENIX, we performed a full sPHENIX detector simulation to demonstrate such capability. The simulation set up includes the following components:

- PYTHIA8 event generation with the configuration in Section 2.1 and all events are generated at (x,y,z)=(0,0,0).
- Full GEANT4 detector response with all the tracking detectors (MVTX + INTT + TPC), which is represented in cylindrical geometry approximations.
- For performance evaluation in Au+Au collisions, hits of PYTHIA8 events are embedded into hits of central Au+Au collisions from HIJING and then input to GEANT4 simulation.
- Track reconstruction with the GENFIT2 package.

From the chain of PYTHIA8 +GEANT4 simulation and track reconstruction, DST files containing all reconstructed tracks are produced. The next analysis step to find secondary vertex is done with these DST files. The RAVE package developed by the CMS collaboration has been adopted in the sPHENIX software, and the GENFIT2 package for generalized Kalman Filter tracking provides interfaces to the RAVE. Therefore, reconstructed tracks with the GENFIT2 can be easily used for vertexing with the RAVE. The analysis step to reconstruct secondary vertex as follows:

- Events containing at least one truth jet of $p_T > 20$ GeV/c in $|\eta| < 0.6$ are used in the secondary vertex finding and flavor tagging of jets is done with the tagger introduced in Section 2.1.
- Only tracks with $\chi^2/ndf < 5$ in each event are used for primary vertex finding and the adaptive method for single vertex (`avf-smoothing:1`) is used.

- For each jet of $p_T > 20$ GeV/c in $|\eta| < 0.6$, reconstructed tracks of $\chi^2/ndf < 5$ within a jet cone ($\Delta R < 0.4$) are used for secondary vertex finding. The adaptive method for multiple vertices (`avr-smoothing:1`) is used.

- Various p_T cuts are used to compare b-jet tagging performance which result in different contamination of soft particles.

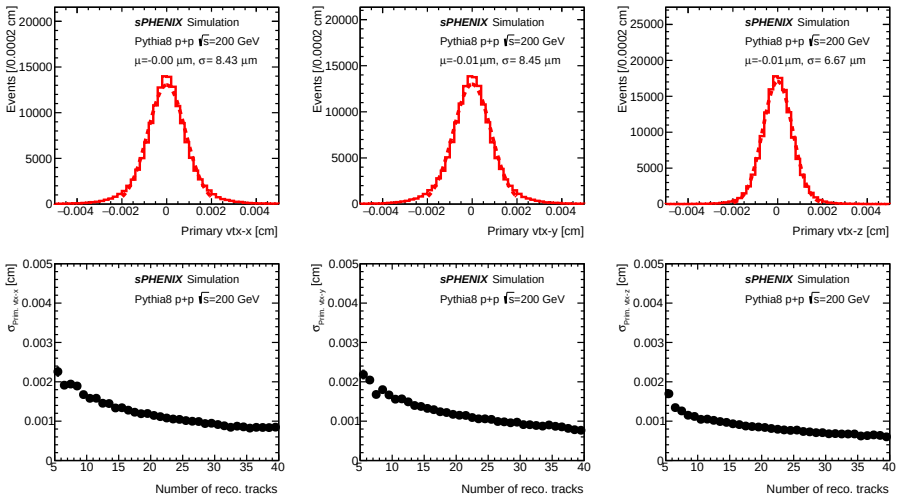

Figure 3.7: Primary vertex resolution of p+p events containing at least one jets of $p_T > 20$ GeV/c in $|\eta| < 0.6$ (top) and the resolution as a function of the number of reconstructed tracks (bottom).

From this procedure, primary and secondary vertices for each event are obtained. The primary vertex resolution of p+p events containing at least one truth jet of $p_T > 20$ GeV/c in $|\eta| < 0.6$ is better than 10 μm in all x, y, and z directions as shown in Figure 3.7. The left panel of Figure 3.8 shows the number of secondary vertices per jet. In case of light jet (black), most of jets have only one secondary vertex, but the chances of having more than one secondary vertex increases in charm and bottom jets which indicates decay vertex of charm and bottom hadrons. Even in light jets, multiple secondary vertices can be found due to decay of light mesons such as K^0. The right panel of Figure 3.8 shows secondary vertex mass of light jets in low mass region with an assumption of tracks being pions, and a clear peak of K^0 is seen. The secondary vertex from K^0 decay can be removed by applying mass cut ($0.47 < M < 0.53$ GeV/c^2) to increase purity of b-jets.

For each secondary vertex in a certain jet, the 3D flight distance from the primary vertex and its significance (distance divided by vertex error) is calculated, and the secondary vertex of most significant deviation is selected. Figure 3.9

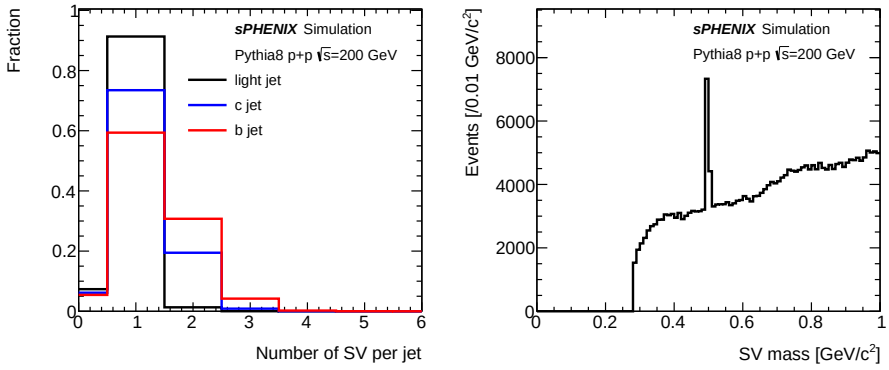

Figure 3.8: The number of secondary vertices per jet (left) and secondary vertex mass distribution from light jet in low mass region (right).

shows the 3D flight distance of the secondary vertex of most significant deviation (left) and its significance (right). Each distribution is normalized to unity. The distributions from b-jets are much broader than the distribution from light jets which is basically due to the decay vertex of long-lived b-hadrons. Based on these plot, the purity and efficiency of b-jet tagging can be evaluated.

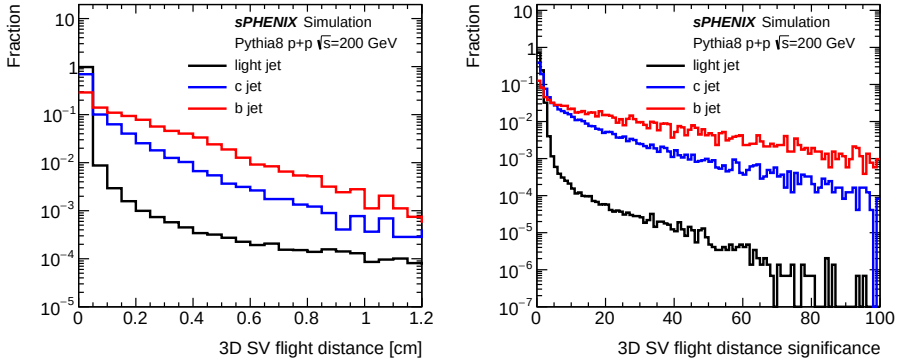

Figure 3.9: The 3D flight distance of the secondary vertex of most significant deviation (left) and its significance (right) for b-jets (red), c-jets (blue) and light jets (black).

3.2.3 Results

Based on the 3D flight distance significance shown in Figure 3.9, b-jets can be enriched by applying a large value of significance cut, but the efficiency decreased. The significance cut can be optimized based on the b-jet purity

and efficiency. Figure 3.10 shows light jet and c-jet efficiency as a function of b-jet tagging efficiency and rejection of different flavor jets as a function of the significance cut of 3D flight distance. Each secondary vertex should contain at least two good associated tracks, and a good associated track is defined as a track of weight in vertex determination is larger than 0.6. With this requirement, secondary vertices from uncorrelated tracks can be reduced. Figure 3.11 shows the same set of plots as in Figure 3.10, but the requirement of minimum number of associated tracks to a secondary vertex is three. When comparing the rejection plots (right) between Figure 3.10 and 3.11, initial rejection of light jets is much larger with the requirement of three minimum associated tracks.

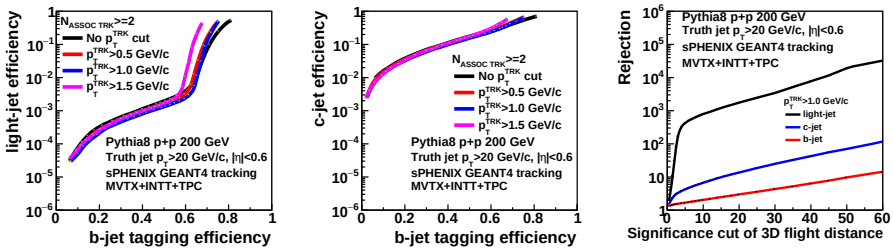

Figure 3.10: The efficiency of light jet (left) and c-jet as a function of b-jet tagging efficiency using secondary vertex method and rejection factors of different flavor jets as a function of significance cut of 3D flight distance of secondary vertex in $p+p$ collisions. It it required to have at least two good associated tracks to each secondary vertex.

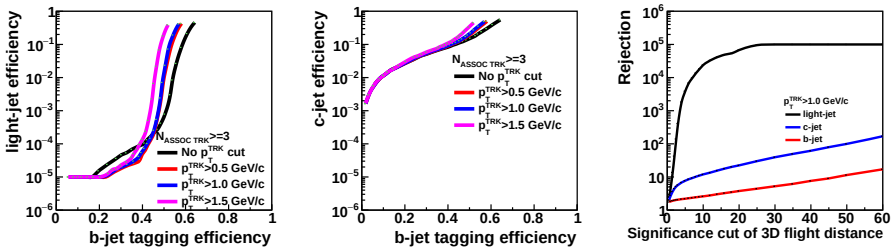

Figure 3.11: The efficiency of light jet (left) and c-jet as a function of b-jet tagging efficiency using secondary vertex method and rejection factors of different flavor jets as a function of significance cut of 3D flight distance of secondary vertex in $p+p$ collisions. It it required to have at least three good associated tracks to each secondary vertex.

Figure 3.12 shows b-jet purity versus efficiency with a requirement of minimum number of good associated tracks of two (left) or three (right). The b-jet purity is defined as a fraction of b-jet to all jets. Similarly with the results from the track counting method shown in Figure 3.4, a higher b-jet purity can be

achieved with a more strict cut, but the efficiency in low b-jet purity becomes lower. Each plot includes four distributions of various p_T cut for tracks. In case of the minimum two associated tracks for a secondary vertex, the distribution of a moderate p_T cut (blue, $p_T > 1$ GeV/c) shows a slightly better performance than the distribution without any p_T cut (black). However, the b-jet efficiency looks better without p_T cut in case of the minimum three associated tracks for a secondary vertex.

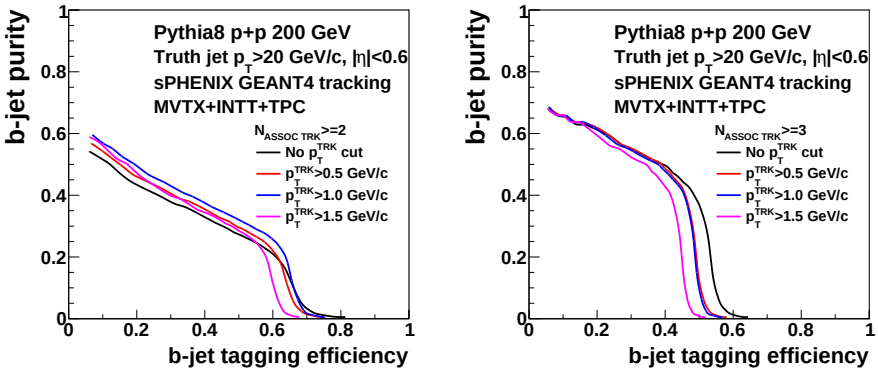

Figure 3.12: b-jet tagging performances in $p+p$ collisions using secondary vertex method.

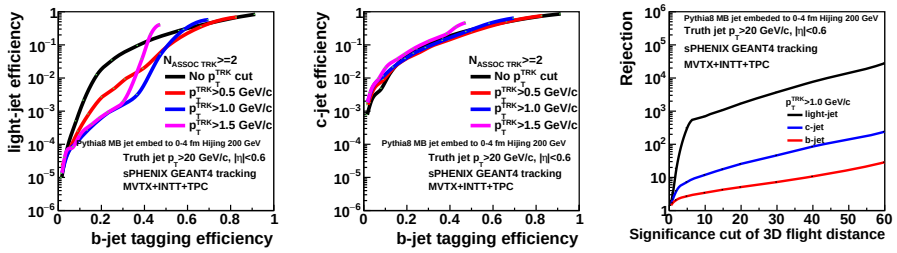

Figure 3.13: The efficiency of light jet (left) and c-jet as a function of b-jet tagging efficiency using secondary vertex method and rejection factors of different flavor jets as a function of significance cut of 3D flight distance of secondary vertex in central Au+Au collisions. It it required to have at least two good associated tracks to each secondary vertex.

In order to evaluate b-jet tagging performance in central Au+Au collisions, PYTHIA8 events are embedded into central Au+Au collision events from HIJING as described in Section 3.2.2. Truth jet finding and flavor tagging are done only with PYTHIA8 events. When finding secondary vertices, background particles from HIJING events around jets from PYTHIA8 events are included. In order to remove background tracks whose contribution is much larger than

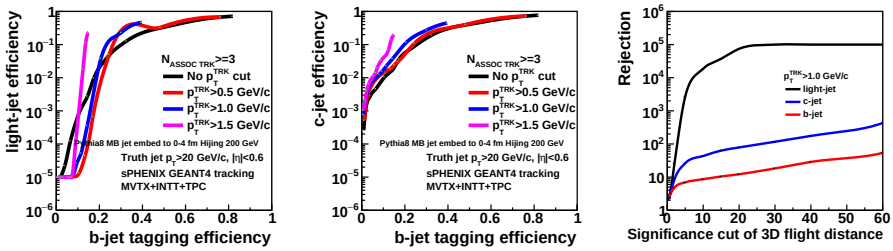

Figure 3.14: The efficiency of light jet (left) and c-jet as a function of b-jet tagging efficiency using secondary vertex method and rejection factors of different flavor jets as a function of significance cut of 3D flight distance of secondary vertex in central Au+Au collisions. It it required to have at least three good associated tracks to each secondary vertex.

those in $p+p$ collisions, a tighter track quality cut ($\chi^2/ndf < 2$) is used. In addition, tracks without MVTX hit are rejected which have a high chance of being fake tracks in high multiplicity circumstance. Figure 3.13 shows the efficiency of light jet and c-jet efficiency as a function of b-jet efficiency and rejection of different flavor jets as a function of significance cut of secondary vertex 3D flight distance with a minimum two associated tracks for each secondary vertex, and Fig. 3.14 show the same set of plots with a minimum three associated tracks for each secondary vertex. Compared to the same plots in $p+p$ collision shown in Fig. 3.10 and 3.11, a tighter significance cut is needed to achieve a similar light jet rejection which results in a worse b-jet efficiency. Figure 3.15 shows the performance of b-jet tagging in central Au+Au collisions using secondary vertex method with minimum two (left) or three (right) associated tracks per secondary vertex. At this moment, b-jet efficiency around 40% b-jet purity is quite low, and we expect to improve the b-jet tagging performance with updated tracking software in near future.

After the initial identification of b-jet candidates, the purity of b-jets in the candidate sample will be quantified in a data-driven way using the invariant mass and transverse momentum of the secondary vertex, which has proven to be critically important in the LHC environment [12, 11]. As shown in Figure 3.16, secondary vertex of b-jet is likely to have higher mass and higher number of associated tracks. These distributions can be used for template fit on the b-jet candidate sample to quantify its purity. For this plot, secondary vertices which 3D flight distance significance is larger than 10 shown in Fig 3.9 and 3.10, and the corresponding b-jet purity is about 35%. This point will be tuned with improved tracking software.

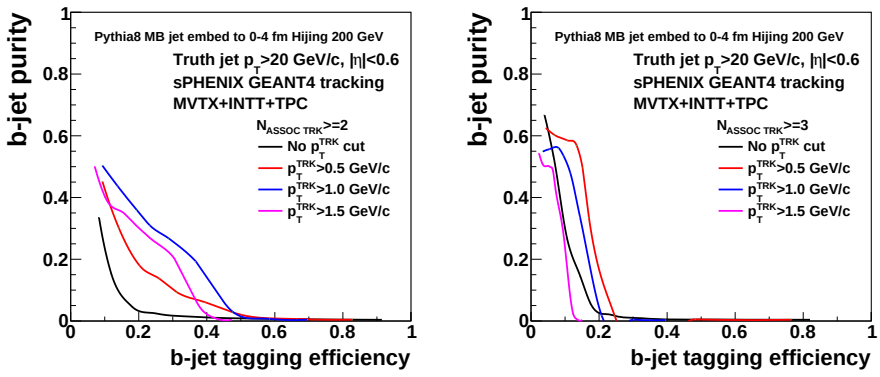

Figure 3.15: b-jet tagging performances in Au+Au collisions using secondary vertex method. The upper limit of all curves from both panels represents the best performance curve using various tunes of the secondary vertex method. We expect improved performance as the tracking software improves.

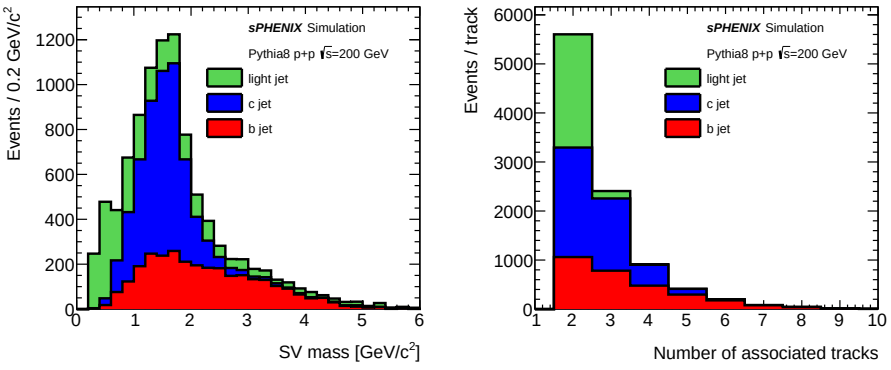

Figure 3.16: Secondary mass (left) and the number of associated tracks (right) distributions of light, c, and b-jets in $p+p$ collisions.

Chapter 4

Correlations of b-jet pairs

4.1 Introduction

Inclusive b-jets can originate from a high-energy b-quark (a true b-quark jet) or from a gluon that splits into a b-quark and b-antiquark ($g \to b\bar{b}$-jet). These two categories of b-jets could potentially have very different interactions with the QGP, because in the latter case the correlated b-quark and b-antiquark traverse coherently through the QGP in a color octet state with twice the b-quark mass [14]. Although inclusive b-jets at RHIC are expected to be dominated by the b-quark jets [18], the remaining $g \to b\bar{b}$-jet component could complicate the interpretation of the inclusive b-jet results.

The fraction of true b-quark jets can also be enhanced by selecting b-quark partonic production channels. sPHENIX will allow us to do so by requiring the b-jet candidate to be correlated with another b-jet, as illustrated in Figure 1.4. In particular, correlations between two b-jets can be measured with high statistics using the MVTX and sPHENIX detectors, taking advantage of their high rate capability and their large instrumented acceptance (covering nearly 80% of produced di-jets [2]).

4.2 Simulation and Analysis Setup

The simulations for the di-b-jet studies uses the same PYTHIA8 configuration file detailed in Section 2.1 with the following exception:

```
PhaseSpace:pTHatMin = 10.0
```

This analysis uses truth jet information only, where the truth jets are reconstructed using the FASTJET anti-k_T algorithm with $R = 0.4$. PYTHIA8 events were first triggered on a b-jet with $p_T > 10$ GeV/c and $|\eta| < 2$ to be used for further analysis and cuts. Approximately 231 pb^{-1} of effective p+p collisions were generated for use in this study. The basic cuts and assumptions used in the analysis are given in Table. 4.1.

Table 4.1: Analysis cut information for di-b-jet study.

	p+p	Au+Au
cuts	$\|\eta_{1,2}\| < 0.7$	
	$p_{T,1} > 20$ GeV/c	
	$p_{T,2} > 10$ GeV/c	
	$\|\Delta\phi_{12}\| > 2\pi/3$	
	$\|z\| < 10$ cm	
b-jet Eff	60%	40%
b-jet Purity	40%	40%
b-jet R_{AA}		0.6

The b-jet efficiency, given in Table 4.1, is applied statistically to each b-jet in the event. It is likely that the tagging efficiency for the 2nd b-jet in the di-b-jet event is significantly higher. However, since we don't have simulation studies of di-b-jet efficiency (or purity), we choose to take the conservative approach. We apply an $R_{AA} = 0.6$ factor only to the leading jet in the di-b-jet, under the argument that, in the simplest approximation, if both jets lose the same fraction of energy in the Au+Au collisions, the number of pair is reduced by R_{AA}. Since this is a pure truth simulation, the effects of the b-jet purity on the pairs are non-trivial to properly estimate. For a conservative projection estimates, we assume that the purity increases the statistical errors by $1/\sqrt{P}$ for each jet, where P is the purity. This effect occurs on both b-jets, and therefore is squared on the di-b-jet measurements. The purity is not applied statistically on a jet-by-jet basis, but rather implemented as a scaling of the statistical uncertainties on the x_j distribution. The work on quantifying the di-b-jet pair purity and efficiency in full GEANT4 simulation is still on-going and the results are expected for the next revision of this study.

After applying the statistical efficiency effects and, in the case of the Au+Au, the R_{AA}, we find the following number of di-b-jet:

- p+p (200 pb^{-1}): 2868
- Au+Au (236 pb^{-1}): 897

In both cases, the distribution of $x_j = p_{T,2}/p_{T,1}$ for b-jet pairs is calculated. The statistical errors on each point are then scaled by $1/P$ to take the effect of the purity into account. In the case of the Au+Au, the statistical errors are additionally scaled by the ratio of the simulated nucleon-nucleon luminosity (236 pb^{-1}) to the desired nucleon-nucleon luminosity for the given centrality bin, given by Table 4.2. The $\langle x_j \rangle$ is then calculated for p+p, and each centrality bin in Au+Au. The resulting uncertainties are shown in Table 4.2.

Table 4.2: The di-b-jet $\langle x_j \rangle$ for p+p and Au+Au collisions at $\sqrt{s_{NN}}$ = 200 GeV.

	N_{evt}	N_{coll}	$\int \mathcal{L}_{nn}\, dt\, [pb^{-1}]$	$\langle x_j \rangle$
p+p	–	–	200	0.724 ± 0.008
Au+Au 0-10%	24.0B	962	549	0.723 ± 0.009
Au+Au 10-20%	24.0B	603	344	0.723 ± 0.011
Au+Au 20-40%	48.0B	296	338	0.723 ± 0.011
Au+Au 40-60%	48.0B	94	107	0.723 ± 0.021
Au+Au 60-92%	76.8B	15	27	0.723 ± 0.042

4.3 Results

A preliminary projection of the transverse momentum balance, x_j, of b-jet pairs is shown in Figure. 4.1 for p+p and 0-10% central Au+Au collisions at $\sqrt{s_{NN}}$ = 200 GeV. These results are comparable in precision with recent results from Pb+Pb collision at $\sqrt{s_{NN}}$ = 5.02 TeV measured by the CMS collaboration [12]. Further, the projected uncertainties on the mean asymmetry, $\langle x_j \rangle$, as a function of N_{coll} is shown in Figure 4.2.

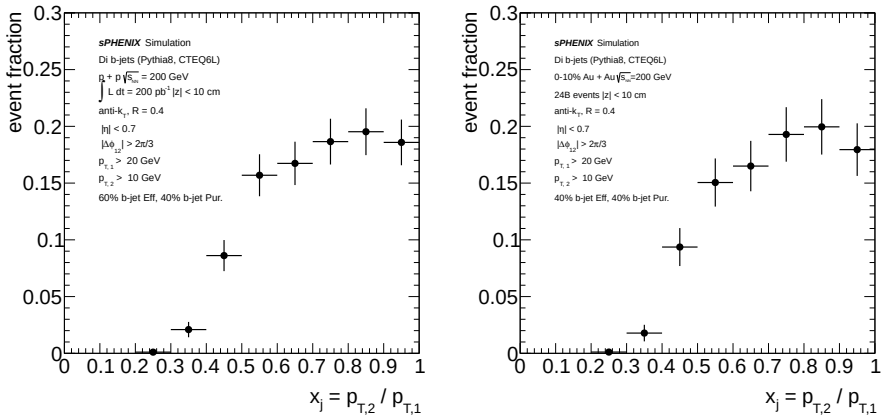

Figure 4.1: Preliminary projection of transverse momentum balance of b-jet pairs as enabled by sPHENIX and the MVTX upgrade, for p+p (left) and for 0-10% central Au+Au collisions at $\sqrt{s_{NN}}$ = 200 GeV (right).

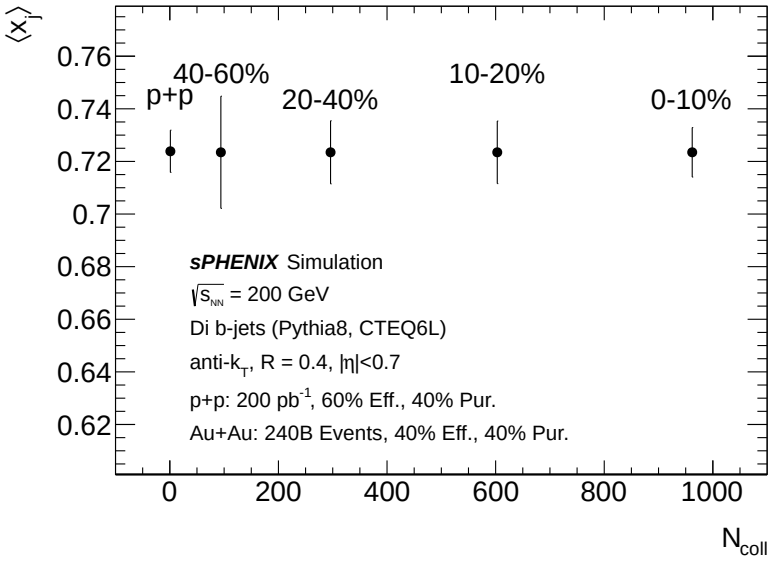

Figure 4.2: The mean di-b-jet asymmetry, $\langle x_j \rangle$ as a function of N_{coll} in p+p and Au+Au collisions at $\sqrt{s_{NN}}$ = 200 GeV.

Chapter 5

Exploring b-jet-B-meson correlations

5.1 Introduction

Inspired by reference [15], in this chapter, we further explore b-jet-B-meson correlation via the non-prompt-D meson decay product from the B-meson. The results are still very preliminary, and are intended for internal discussion within the collaboration. Meanwhile, we would like to use this exploratory study to demonstrate new probes enabled by combining high precision tracking and high rate jet detector at RHIC.

Besides the di-b-jet correlation studies as discussed in the last chapter, we further study the b-jet-B-meson correlations with the B-meson within either the leading or the away-side b-jet. Such process can help understand the b-quark $\rightarrow$ B-meson fragmentation process and extend the away-side transverse momentum coverage down to $p_T = 0$. The b-jet and B-meson correlations can provide the information of how b quark lose energy along its traversing path in the QGP. It is sensitive to modifications of b quark parton shower and fragmentation process in the hot and dense QGP medium, and further help separate the collisional energy loss or radiative energy loss.

As this study can tag the partonic kinematics of the D meson, it would also help understand the origin of non-prompt-D meson, and help the interpretation of the single non-prompt-D meson study as also performed by the HF topical group.

To initiate this study, this note currently focuses on studying the b-jet-B-meson correlations with the away side pairs from the $B \rightarrow D \rightarrow \pi K$ decay chain in PYTHIA8 truth information, in order to estimate the signal yield. We are working on quantifying the signal purity and efficiency via GEANT4 based simulation to produce a realistic projection on the significance of this measurement. Further more, although not discussed in this note, the analysis techniques developed from this study allow the search of prompt-D-meson tagged jets,

which will provide the information about c-jets, formation of Charmed hadrons, and help understand the mass/flavor dependent parton energy loss mechanisms.

5.2 Simulation and Analysis Setup

As a first step of this study, 18M PYTHIA8 Hard QCD simulation events were used to estimate the cross section. Only events containing leading truth b-jets with $p_T > 20$GeV/c and within $|\eta| < 1.0$ are used in this analysis. For non-prompt D-meson reconstruction, we focus on the $D^0 \rightarrow \pi K$ decay channel. PYTHIA8 truth charged kaons and pions with $p_T > 0.3$ GeV/c, $|\eta| < 1.0$ and originated from a displaced vertex are used in this study. In addition, charged pions and kaons candidates are required to be within away-side region of the leading b-jet ($|\Delta\varphi| > \frac{2}{3}\pi$). To form the charge neutral D-meson candidates, pairs of kaon and pion are required to have opposite charge sign, and the differences between their decay vertex-z component should be within 100 microns. For the preliminary result of this study, we use the truth information recorded in the PYTHIA8 simulation. Kaons and pions should come from the same D-meson decay and the D-meson should be the decay product of a B-meson. Another case included in the analysis sample is that the D-meson is the decay product of another D-meson from a B-meson decay. The luminosity is based on sPHENIX continuous run from 2022 to 2027 projection which results in 240B MB Au+Au collisions without requiring a Au+Au trigger [17]. The physical projection scales the distributions in PYTHIA8 simulation with the N_{coll} in MB (0-100%) Au+Au collisions and the total projected luminosity.

Since a different PYTHIA8 sample than that in Section 2.2 is used in this b-jet and non-prompt D-meson correlations study, a cross-check is done to study the inclusive jet and inclusive b-jet relative yields as shown in Figure. 5.1. A consistent result is achieved between this study and the early studies as shown in Figure. 2.1. For the detector response part, assumption is made about the b-jet tagging efficiency as 0.5 and its purity as 1, and the b-jet purity with away-side tagged B-meson needs further quantification. According to the B-meson and non-prompt D-meson studies, the non-prompt D-meson reconstruction efficiency is assumed as 0.6 and its purity as 1. Further studies will also include a more realistic purity determined from a fast simulation with pre-determined detector resolutions from a full GEANT4 simulation.

5.3 Results (Internal discussion use only)

The observable is defined as the ratio between the transverse momentum of the non-prompt D-meson and the transverse momentum of the leading b-jet, z_j. A preliminary projection of the transverse momentum balance of a leading b-jet and an away-side non-prompt D-meson correlations in 240B MB Au+Au collisions is shown in Figure. 5.2.

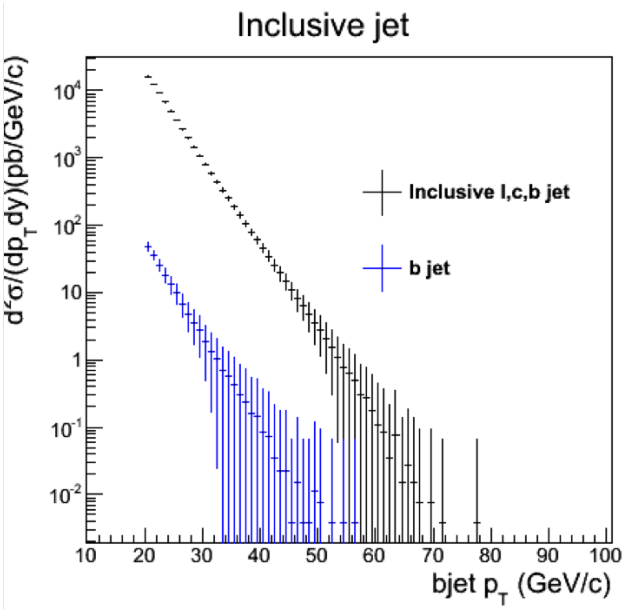

Figure 5.1: Cross check the PYTHIA8 sample used in the b-jet-B-meson study by estimating the cross section of inclusive jets and b-jets in 200 GeV p+p collisions, which is consistent with Figure. 2.1.

With the same luminosity of 200 GeV Au+Au collisions, the preliminary result of the azimuthal correlations between a leading b-jet and an away-side B-meson is shown in the left panel of Figure 5.3 and the correlations between a leading b-jet and an away-side non-prompt D-meson is shown in Figure 5.3.

Since the purity for the b-jet and B-meson are assumed to be 100%, these preliminary results only represent the max statistics significance we could obtain. Therefore, Figure 5.2 and 5.3 are not to be used in external showing, while the purity quantification via simulation is being performed.

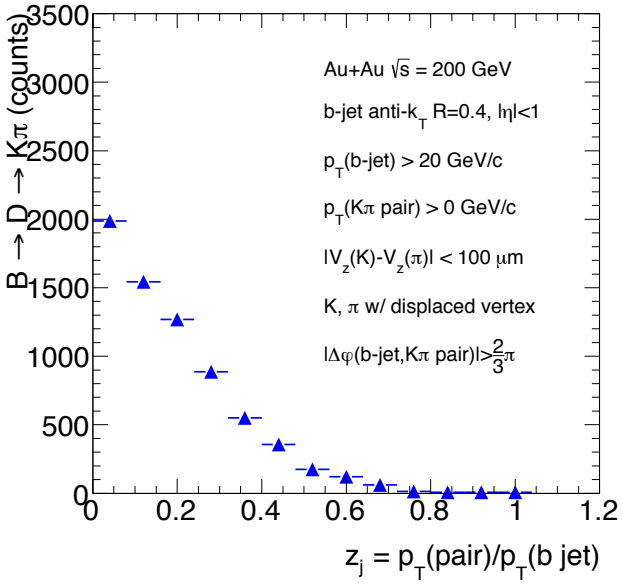

Figure 5.2: For internal discussion only: preliminary projection of transverse momentum balance of b-jet and non-prompt D-meson correlations in 240B MB Au+Au collisions (0-100% centrality) at $\sqrt{s_{NN}} = 200$ GeV. A R_{AA} of 0.6 is assumed without a p_T dependence. As purity is still under study, this projection assumed 100% purity for both D-meson and b-jet. Therefore, it gives the upper limit of the statistical significance.

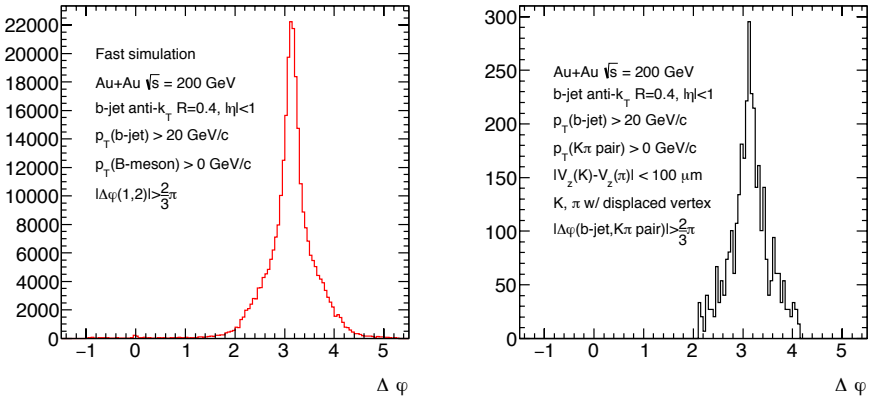

Figure 5.3: For internal discussion only: preliminary projection of azimuthal correlations between a leading b-jet and an away-side B-meson (left) or non-prompt-$D \rightarrow \pi K$ (right) in 240B MB (0-100% centrality) Au+Au collisions at $\sqrt{s_{NN}} = 200$ GeV. The B-meson channel is not measured, but represent the source distribution for the non-prompt-D observables. Note, the B-meson channel has much higher statistics as the non-prompt-$D \rightarrow \pi K$, as the later case suffer from the branching ratio of the decay chain. As purity is still under study, this projection assumed 100% purity for both D-meson and b-jet. Therefore, it gives the upper limit of the statistical significance.

Chapter 6

Final words

This note is a snapshot of the HF-jet studies performed by the HF topical group. We demonstrated the capability of tagging b-jet using the sPHENIX with MVTX upgrade in p+p and central Au+Au environment using GEANT4 simulation and reconstruction. MVTX upgrade is critical in enabling the b-jet capability. The projection for b-jet nuclear modification and di-b-jet correlation are then presented. In the end, the progress of exploring the b-jet-B-meson correlations is discussed.

Work is on-going to update these studies with the in-development new tracking software and to improve the purity studies via simulation. Many more topics are also open for volunteers, as discussed in the Heavy Flavor Topical Group Wiki

Bibliography

[1] The RAVE/VERTIGO vertex reconstruction toolkit and framework. 3.1.2

[2] A. Adare et al. An Upgrade Proposal from the PHENIX Collaboration. 2015. 1.1, 1.2, 1.2.2, 1.4, 3.1.1, 4.1

[3] A. Adare et al. Centrality-dependent modification of jet-production rates in deuteron-gold collisions at $\sqrt{s_{NN}}$=200 GeV. *Phys. Rev. Lett.*, 116(12):122301, 2016. 2.2, 2.1

[4] Yasuyuki Akiba et al. The Hot QCD White Paper: Exploring the Phases of QCD at RHIC and the LHC. 2015. 1.1

[5] Nestor Armesto, Carlos A. Salgado, and Urs Achim Wiedemann. Medium induced gluon radiation off massive quarks fills the dead cone. *Phys. Rev.*, D69:114003, 2004. 1.1

[6] Andrea Banfi, Gavin P. Salam, and Giulia Zanderighi. Accurate QCD predictions for heavy-quark jets at the Tevatron and LHC. *JHEP*, 07:026, 2007. 1.1

[7] Matteo Cacciari, Stefano Frixione, and Paolo Nason. The p(T) spectrum in heavy flavor photoproduction. *JHEP*, 03:006, 2001. 1.1, 2.2, 2.1

[8] Matteo Cacciari, Mario Greco, and Paolo Nason. The P(T) spectrum in heavy flavor hadroproduction. *JHEP*, 05:007, 1998. 1.1, 2.2, 2.1

[9] Matteo Cacciari and Gavin P. Salam. Dispelling the N^3 myth for the k_t jet-finder. *Phys. Lett.*, B641:57–61, 2006. 2.1

[10] Matteo Cacciari, Gavin P. Salam, and Gregory Soyez. FastJet User Manual. *Eur. Phys. J.*, C72:1896, 2012. 2.1

[11] Serguei Chatrchyan et al. Evidence of b-Jet Quenching in PbPb Collisions at $\sqrt{s_{NN}} = 2.76$TeV. *Phys. Rev. Lett.*, 113(13):132301, 2014. [Erratum: Phys. Rev. Lett.115,no.2,029903(2015)]. 1.1, 1.4, 1.4, 3.1.3, 3.6, 3.2.3

[12] CMS Collaboration. Transverse momentum balance of b-jet pairs in PbPb collisions at 5 TeV. 2016. 1.1, 1.4, 1.4, 3.2.3, 4.3

[13] Yuri L. Dokshitzer and D. E. Kharzeev. Heavy quark colorimetry of QCD matter. *Phys. Lett.*, B519:199–206, 2001. 1.1

[14] Jinrui Huang, Zhong-Bo Kang, and Ivan Vitev. Inclusive b-jet production in heavy ion collisions at the LHC. *Phys. Lett.*, B726:251–256, 2013. 1.1, 1.4, 2.1, 2.3, 2.2, 4.1

[15] Jinrui Huang, Zhong-Bo Kang, Ivan Vitev, and Hongxi Xing. Photon-tagged and B-meson-tagged b-jet production at the LHC. *Phys. Lett.*, B750:287–293, 2015. 1.4, 5.1

[16] Ming X. Liu et al. A monolithic-active-pixel-sensor-based vertex detector (mvtx) for the sphenix experiment at rhic, a pre-proposal of. 2017. 1.1

[17] Jamie Nagle and Dennis Perepelitsa. sphenix five-year (2022-2026) running scenario and luminosity projections. 2017. 1.3, 5.2

[18] E. Norrbin and T. Sjostrand. Production and hadronization of heavy quarks. *Eur. Phys. J.*, C17:137–161, 2000. 1.4, 4.1

[19] C. Patrignani et al. Review of Particle Physics. *Chin. Phys.*, C40(10):100001, 2016. 1.1

[20] J. Pumplin, A. Belyaev, J. Huston, D. Stump, and W. K. Tung. Parton distributions and the strong coupling: CTEQ6AB PDFs. *JHEP*, 02:032, 2006. 2.1

[21] J. Pumplin, D. R. Stump, J. Huston, H. L. Lai, Pavel M. Nadolsky, and W. K. Tung. New generation of parton distributions with uncertainties from global QCD analysis. *JHEP*, 07:012, 2002. 2.1

[22] Johannes Rauch and Tobias Schlter. GENFIT a Generic Track-Fitting Toolkit. *J. Phys. Conf. Ser.*, 608(1):012042, 2015. 1.2.1

[23] Torbjorn Sjostrand, Stephen Mrenna, and Peter Z. Skands. PYTHIA 6.4 Physics and Manual. *JHEP*, 05:026, 2006. 1.1, 2.1

[24] Torbjorn Sjostrand, Stephen Mrenna, and Peter Z. Skands. A Brief Introduction to PYTHIA 8.1. *Comput. Phys. Commun.*, 178:852–867, 2008. 2.1

[25] T. Speer, Kirill Prokofiev, R. Fruhwirth, W. Waltenberger, and P. Vanlaer. Vertex fitting in the CMS tracker. 2006. 3.1.2

[26] Wolfgang Waltenberger. *Development of Vertex Finding and Vertex Fitting Algorithms for CMS*. PhD thesis, Vienna, Tech. U., 2004. 3.1.2